

“Split Brick by Qigong” and a Probe into Its Mechanics Problem

Zhou Danfa^{1*}, Ji Wenjie², Huang Boen³, Pei Houju¹, Li Xinpeng⁴

1. College of Aerospace Engineering, Nanjing University of Aeronautics and Astronautics, Nanjing 210016, P. R. China;

2. National Microgravity Laboratory, Institute of Mechanics, Chinese Academy of Sciences, Beijing 100190,

P. R. China and School of Engineering Sciences, University of Chinese Academy of Sciences, Beijing 100049, P. R. China;

3. Shanghai Electro-Mechanical Engineering Institute, CASC, Shanghai 201109, P. R. China;

4. Chengdu Aircraft Industrial(Group)Co Ltd, AVIC, Chengdu 610000, P. R. China

(Received 20 March 2018; revised 20 April 2018; accepted 30 May 2018)

Abstract: Based on the phenomenon of “split brick by Qigong”, a mechanical model for short beam impact is proposed. Combined with the traditional energy method, a theoretical analysis of the impact of the short beam (Timoshenko beam) closer to the real situation is made considering the quality and initial deformation. The optimal solution of short beam impact problem of how to choose the position where the short beam is most likely to break is obtained. The finite element numerical analysis and experimental test are used, and the results verify the applicability of the theoretical analysis of the proposed model.

Key words: solid mechanics; split brick by Qigong; cantilever beam; impact

CLC number: O348.7 **Document code:** A **Article ID:** 1005-1120(2018)S-0096-07

0 Introduction

As one of China’s intangible cultural heritage, “Qigong” has a very long history. The literatures on mechanical research of the phenomenon “Split brick by Qigong” and how to choose the optimal impact location that makes the brick easiest to break is rare at home and abroad. In this paper, this phenomenon is simplified to the problem of cantilever beam impact, and the beam quality and initial deformation effects are taken into account to study its mechanical characteristics and the best impact position for the exploration of the broken (failure) of the bricks. A general conclusion of the problem of cantilever beam impact is drawn, so that it has more engineering application value^[1].

1 Theoretical Analysis

1.1 Basic assumption

The establishment and analysis of the model are based on the following assumptions:

(1) The impact collision is a completely inelastic collision, the energy absorbed by a shock body during impact is not considered.

(2) The impact stress of the beam is within the elastic range, the stiffness and elastic constants during impact are the same as those of static load^[2].

1.2 Model establishment

The essence of the phenomenon “Split brick by Qigong” is to hit a brick by a certain force at a certain speed. In the process of “split brick”, one end of the brick is fixed, and the other end is free, which can be simplified as an impact problem of a cantilever beam. The impact model is shown in Fig. 1, where m is the mass of the shock body, l the extension of the beam, and a (distance from the constraint) the coordinate of the impact position. In the conditions consistent with the above assumptions, the speed at which the shock body and the beam are initially approached is v , the initial speed at which the two start to

* Corresponding author, E-mail address: dfazhou@163.com.

How to cite this article: Zhou Danfa, Ji Wenjie, Huang Boen, et al. “Split brick by Qigong” and a probe into its mechanics problem[J]. Trans. Nanjing Univ. Aero. Astro., 2018, 35(S): 96-102.

<http://dx.doi.org/10.16356/j.1005-1120.2018.S.096>

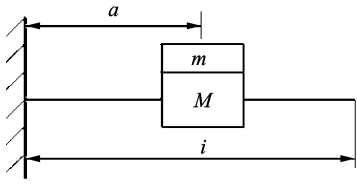


Fig. 1 Diagram of impact model

move together is v_1 , the sum kinetic powers of the two is T , which can be considered as the effective kinetic energy transformed into the deformation energy of the beam, M is the equivalent mass defined by the kinetic energy of the beam^[3], that is, the kinetic energy of the concentrated mass M at the impact position is equal to the kinetic energy of the whole beam. M can be obtained from the function of the initial velocity distribution of the beam.

The relationship of T can be written as

$$T = \frac{1}{2}(M+m) \left(\frac{mv}{M+m} \right)^2 = \frac{m^2 v^2}{2(M+m)} \quad (1)$$

The beam is simplified as a linearly elastic body. The diagram of the initial deformation of the beam is shown in Fig. 2.

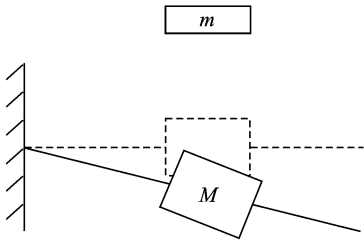


Fig. 2 Diagram of initial deformation of beam

According to the energy conversion during the impact process, after the collision, the kinetic and gravitational potentials of the two concentrated mass are transformed into the deformation energy of the beam, which can be expressed with

$$T + (M+m)g(\Delta_d - \Delta_j) + V_{z_0} = \frac{1}{2}F_d\Delta_d \quad (2)$$

where Δ_d is the dynamic deflection of the beam at the impact position, Δ_j the static deflection of the beam at the impact position caused by its own weight^[4], and V_{z_0} the initial deformation energy of the beam resulted by its own weight. For a linearly elastic body

$$\frac{F_d}{\Delta_d} = \frac{M'g}{\Delta_j} = k \quad (3)$$

where k is the stiffness coefficient of the beam^[5], M' the equivalent mass defined by potential energy, and g the gravity acceleration.

Substituting Eq. (1) and Eq. (3) into Eq. (2), Eq. (4) can be obtained

$$\Delta_d^2 - \frac{2(M+m)}{M'}\Delta_d\Delta_j + \frac{2(M+m)}{M'}\Delta_j^2 - 2V_{z_0}\frac{1}{M'g}\Delta_j - \frac{m^2v^2}{M'g(M+m)}\Delta_j = 0 \quad (4)$$

It is assumed that

$$A = \frac{2(M+m)}{M'} \quad (5)$$

$$B = \frac{m^2v^2}{M'g(M+m)} + \frac{2V_{z_0}}{M'g}$$

So Eq. (4) can be simplified as

$$\Delta_d^2 - A\Delta_d\Delta_j + A\Delta_j^2 - B\Delta_j = 0 \quad (6)$$

The solution is

$$\Delta_d = \frac{A}{2} \left[1 + \sqrt{1 + 4\left(\frac{B}{A^2\Delta_j} - \frac{1}{A}\right)} \right] \Delta_j = K_d\Delta_j \quad (7)$$

where K_d is the dynamic load factor^[6]. For an impact issue

$$\sqrt{4\left(\frac{B}{A^2\Delta_j} - \frac{1}{A}\right)} \gg 1, \frac{B}{A^2\Delta_j} \gg \frac{1}{A} \quad (8)$$

So the approximate solution of K_d is

$$K_d \approx \frac{A}{2} \sqrt{\frac{4B}{A^2\Delta_j}} = \sqrt{\frac{B}{\Delta_j}} = \sqrt{\frac{1}{M'g\Delta_j} \left(\frac{m^2v^2}{M+m} + 2V_{z_0} \right)} \quad (9)$$

For short beams with concentrated loads, the points on the upper surface and the neutral layer are easiest to break. The stress of these points is^[7]

$$\sigma_{st} = \frac{Fa}{w} = \frac{6Fa}{bh^2}$$

$$\tau_{st} = \frac{3F}{2bh} \quad (10)$$

where h is the depth of the beam and b the width of the beam.

As can be seen from the above correlation, the value of σ_{st} and τ_{st} is related to a :

(1) For $13.25 \text{ mm} = h/4 \leq a < l = 180 \text{ mm}$, $\sigma_{st} \geq \tau_{st}$.

The maximum dynamic stress on the upper surface is

$$\sigma_d = K_d \sigma_{st} = \frac{6M'gaK_d}{bh^2} =$$

$$\frac{6}{bh^2} \sqrt{\frac{M'g}{\Delta_j} \left(\frac{m^2 v^2}{M+m} + 2V_{z0} \right)} a^2 = \sqrt{f(a)} \quad (11)$$

where

$$f(a) = \left(\frac{6}{bh^2} \right)^2 \frac{M'g}{\Delta_j} \left(\frac{m^2 v^2}{M+m} + 2V_{z0} \right) a^2 \quad (12)$$

(2) For $0 \text{ mm} < a < h/4 = 13.25 \text{ mm}$, $\tau_{st} >$

σ_{st} .

The dynamic stress of the neutral layer is

$$\tau_d = K_d \tau_{st} = \frac{3FK_d}{2bh} =$$

$$\frac{3}{2bh} \sqrt{\frac{M'g}{\Delta_j} \left(\frac{m^2 v^2}{M+m} + 2V_{z0} \right)} a^2 = \sqrt{\varphi(a)} \quad (13)$$

where

$$\varphi(a) = \left(\frac{3}{2bh} \right)^2 \frac{M'g}{\Delta_j} \left(\frac{m^2 v^2}{M+m} + 2V_{z0} \right) a^2 \quad (14)$$

Eq. (15) can be obtained according to the deflection formula and potential equivalence^[8].

$$\Delta_j = \frac{M'ga^3}{3EI} \left[1 + \frac{3}{5} (1 + \mu) \frac{h^2}{a^2} \right] \quad (15)$$

Eq. (16) can be obtained according to the kinetic equivalence and the velocity distribution of the beam.

$$\frac{1}{2} M v_1^2 = \int_0^l \frac{1}{2} \rho b h v^2(x) dx \quad (16)$$

or

$$M = \rho b h \int_0^l \left(\frac{w}{w_a} \right)^2 dx \quad (17)$$

Considering that the function of velocity distribution of the beam has a similar form with its principal mode, a function that satisfies the boundary condition is used as the principal function^[9-10]. It is assumed that $w = (x)^2$, so

$$M = \rho b h \int_0^l \left(\frac{x}{a} \right)^2 dx = \frac{\rho b h l^3}{3a^2} \quad (18)$$

The initial deformation energy can be calculated by Eq. (19)

$$V_{z0} = \int_0^l \frac{M^2(x)}{2EI} dx + \int_0^l \frac{kF_s^2(x)}{2GA} dx \quad (19)$$

The function of $\sqrt{f(a)}$ and $\sqrt{\varphi(a)}$ can be determined by substituting Eqs. (15), (16), (18), (19) to Eqs. (11), (13), so the maximum value of σ_d and τ_d can be obtained.

2 Numerical Examples

The calculation parameters are as follows:

$m = 10 \text{ kg}$, $H = 150 \text{ mm}$, $v = 1.732 \text{ m/s}$, $b = 115 \text{ mm}$, $h = 53 \text{ mm}$, $l = 180 \text{ mm}$, $\rho = 1900 \text{ kg/m}^3$, $\mu = 0.21$, $E = 5800 \text{ MPa}$, $G = 2400 \text{ MPa}$ ^[11].

Based on the above parameters, the value of V_{z0} , I , M can be obtained, respectively.

$$V_{z0} = \left(\frac{l^5}{40EI} + \frac{l^3}{5GA} \right) q^2 = 8.724 \times 10^{-6} \text{ (J)}$$

$$I = \frac{1}{12} b h^3 = 1.427 \times 10^{-6} \text{ (m}^4\text{)}$$

$$M = \frac{\rho b h l^3}{3a^2} = \frac{0.0225}{a^2} \text{ (kg)}$$

For $13.25 \text{ mm} \leq a < 180 \text{ mm}$

$$f(a) = \frac{3.45 \times 24829.8 \times 10^8}{a + 2.039 \times 10^{-3}/a} \cdot$$

$$\left(\frac{300}{0.0225/a^2 + 10} + 1.744 \times 10^{-5} \right)$$

The function curve of $\sigma_d = \sqrt{f(a)}$ is drawn by software MATLAB (Fig. 3). As shown in Fig. 3, the maximum value of σ_d is 42.46 MPa with $a = 80.3 \text{ mm}$, when the beam is impacted in this position, the beam is most easily broken.

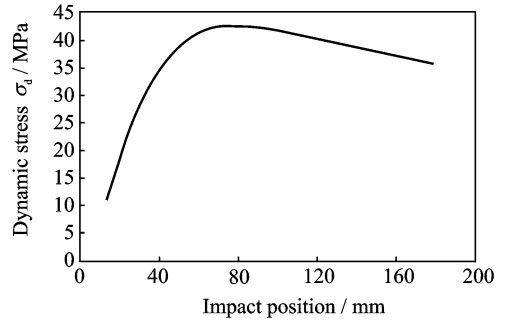


Fig. 3 The function curve of $\sigma_d = \sqrt{f(a)}$

For $0 < a < 13.25 \text{ mm}$

$$\varphi(a) = \frac{6.057 \times 24829.8 \times 10^4}{a^2 (a + 2.039 \times 10^{-3}/a)} \cdot$$

$$\left(\frac{300}{0.0225/a^2 + 10} + 1.744 \times 10^{-5} \right)$$

The function curve of $\tau_d = \sqrt{\varphi(a)}$ is drawn by software MATLAB (Fig. 4).

From Fig. 3, we can know that the beam is most easily broken with impact position $a = 80.3 \text{ mm}$ within the range of $13.25 \text{ mm} < a < 180 \text{ mm}$. Within the range of $0 < a < 13.25 \text{ mm}$, because the region is in the Saint-Venant influence area, the theoretical solution contains a certain deviation from Fig. 4. This issue will not be discussed in detail in this paper.

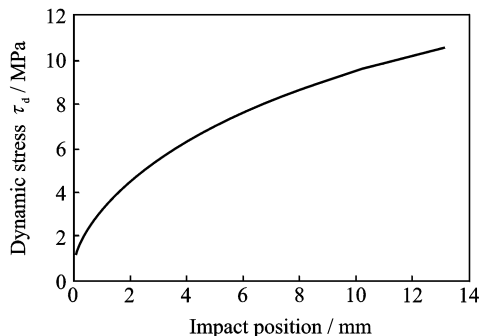


Fig. 4 The function curve of $\tau_d = \sqrt{\varphi(a)}$

3 Numerical Simulation and Analysis Based on Ansys

3.1 Development of finite element model

The model of the brick and the shock body wedge hammer is shown in Fig. 5. The SOLID entity unit supported by ABAQUS is used in the model^[12]. In the experiment, one end of the brick is fixed by surface-surface contact in a clamping area. So in the finite element model, the solid element at the left side of the extension part of the brick is constrained completely to achieve the fixed constraint of the clamping area at the end. The initial velocity of the hammer is in the nega-

tive direction of Y, and its value is 1.732 m/s. The solution time is set to 1.2 ms^[13-14]. All the calculated parameters are the same as those in Section 2.

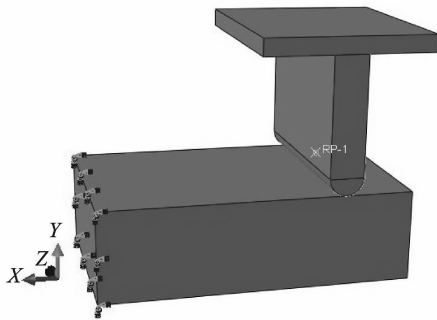


Fig. 5 Finite element model of wedge-hammer

3.2 Results and analysis

The stress distribution of the brick is studied when the hammer hit the different position with the same energy. The brick is divided into some pieces along the X direction at every 10 mm. Three of these simulation results are shown in Figs. 6—8.

According to the data obtained from the simulation, the stress at the impact position and the root of the brick are shown in Table 1.

Table 1 The maximum stress at the root of brick

Impact position/mm	30	40	50	60	70	80	90	100	110	120	130	140
The maximum stress / MPa	26.8	37.3	44.9	48.7	53.5	55.2	51.8	43.7	44.5	41.1	36.6	29.8

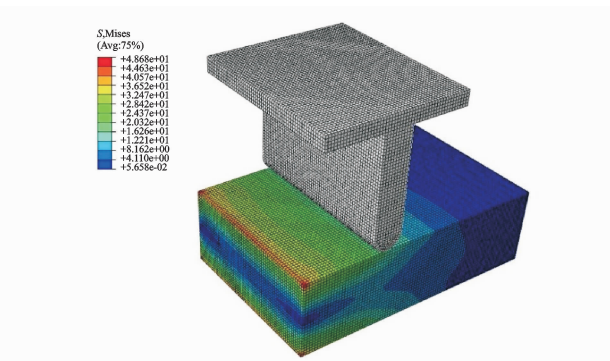


Fig. 6 Stress distribution of brick when the hammer hits the different position (X=60 mm) with the same energy

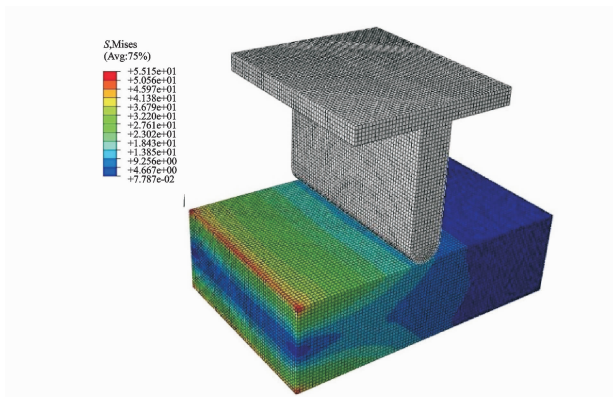


Fig. 7 Stress distribution of brick when the hammer hits the different position (X=80 mm) with the same energy

A curve is fitted according to these figures in Fig. 9.

The data in Table 1 and the curve in Fig. 9

are very consistent with the analytical solution of the theoretical model.

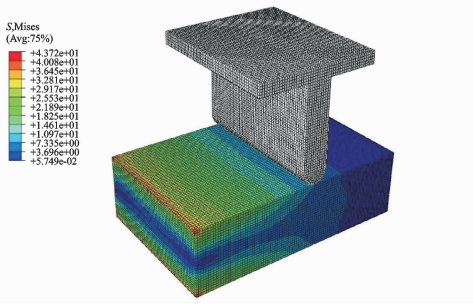


Fig. 8 Stress distribution of brick when the hammer hits the different position ($X = 100$ mm) with the same energy

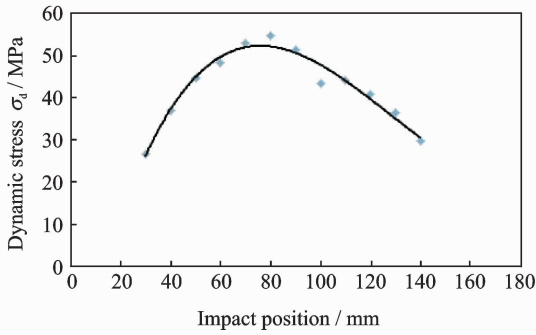


Fig. 9 Fitting curve of the maximum stress at the root of brick

4 Experimental Verification

4.1 Introduction to experimental device

The experimental device consists of guide rail, base, heavy hammer and fasteners. The guide rail is welded to the base and the fasteners are connected to the base by bolt positioning holes^[15]. Fig. 10 is the three views drawing of the experimental device and Fig. 11 is the physical diagram of experimental device.

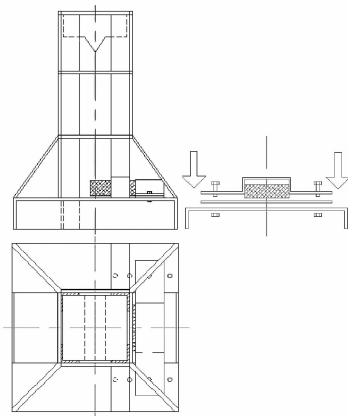


Fig. 10 Three-view drawing of experimental device



Fig. 11 Experimental device photographed

4.2 Results and analysis

In the experiment, we set two impact heights, 150 mm and 100 mm, respectively. Four impact Positions A, B, C, D are selected on the brick (Fig. 12), and the distance from the constraint face are 30 mm, 60 mm, 90 mm, 120 mm, respectively^[16].

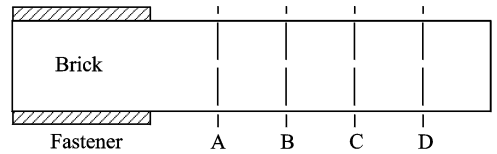


Fig. 12 Diagram of the impact position

Twenty tests are conducted at each impact location with the same impact height, the experimental data are listed in Table 2.

Table 2 Experimental data

Impact height/mm	Impact position/mm			
	30	60	90	120
150	19	14	4	2
100	11	4	1	1

The relation between the number of fractures and the impact location is shown in Fig. 13.

4.3 Experimental conclusions

As shown in Table 2, the closer the impact point to the restraint position, the easier the brick to be broken. For example, when the impact height is 150 mm, there are 95% broken bricks at the impact Position A, while there are only 10% broken bricks at the impact Position D. In the

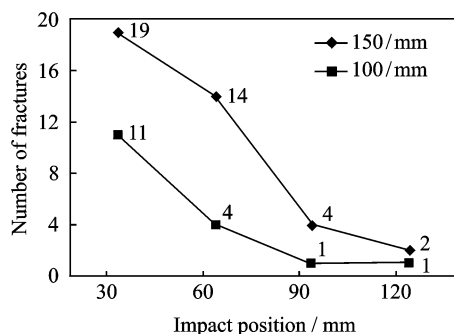


Fig. 13 Relationship between the number of fractures and impact position

broken bricks, the fracture position basically appears at the root of the bricks. Besides, the higher the impact height, the more number of broken bricks. But, when the impact height reaches a certain height, the impact position can be neglected, and the bricks will be all broken.

5 Conclusions

From numerical and simulation analysis, as well as experimental results, some general observations of this study can be summarized as follows:

(1) When the impact position is close to the root of the brick, the broken is mainly caused by shear stress; on the contrary, bending stress is the main reason for the broken.

(2) The brick is most easily broken with the impact position $a = 80.3$ mm within the range of $h/4 < a < l$ for the example cited in this paper.

(3) The simulation results are very consistent with the analytical solution of the theoretical model, which shows that the theoretical model is reasonable and applicable.

(4) According to the experimental result, the fracture position basically appears at the root of the beam in such impact problems.

Acknowledgement

This work was supported in part by the National College Students Innovation Training Program.

References:

[1] AT K, JANI R, JN R. Exact microstructure-dependent Timoshenko beam element[J]. International

Journal of Mechanical Sciences, 2016, S111/112: 35-42.

[2] MEI Z H. Impact strength of equal strength simple beam in consideration of mass[J]. Mechanics and Engineering, 1984(3):28-30.

[3] WANG L H, WANG D, LI R L. Nominal mass of determinate beams [J]. Journal of Shandong University of Technology, 1994, 24(4):389-392.

[4] HE M. Extended model of beam with overhang and its calculation of static deflection and discussion[J]. Journal of Anqing Teachers College, 2014, 20(1):9-11.

[5] HUANG Qiao, LI Wenxian, WANG Bing. Analytical method of steel-concrete composite beam based on interface slip and shear deformation[J]. Journal of Nanjing University of Aeronautics & Astronautics, 2018, 50(1):131-137. (in Chinese)

[6] ZHOU R Y. Discussion on the dynamic load factor of the impact rod considered the mass[J]. Mechanics and Practice, 1997, 19(3):28-30.

[7] LIU H W, LIN J X, CAO M L, et al. Mechanics of materials[M]. 5th ed. Beijing: Higher Education Press, 2010.

[8] TIMOSHENKO S P, GERE J M. Mechanics of materials[M]. New York: Van Nostrand Reinhold Co., 1972.

[9] ZHANG X Z, JI G M. Research on the impact loadings constant of the beam[C]//Specialized Committee, China Mechanical Society, Structural Engineering—A Collection of Papers on the Eighth National Academic Conference on Structural Engineering(3). Beijing: Tsinghua University Press, 1999: 583-587.

[10] XING Y F, XIE W J, ZHU D C. Influence of thickness effects on impact responses of beam[J]. Theoretical and Applied Mechanics, 2004(2):184-190.

[11] LIU G Q, SHI C X, LIU Y B. Analyses of the elastic modulus values of masonry[J]. Journal of Hunan University(Natural Sciences), 2008(4):29-32.

[12] WU J H, LI T, LIU F F, et al. Finite element dynamic simulation of rubbing beam under impact loading[J]. Mining & Processing Equipment, 2010, 38(23):46-48.

[13] SUI Xin, DING Qian. Numerical analysis of dry friction-induced vibration of moving slider-elastic annular beam system[J]. Transactions of Nanjing University of Aeronautics and Astronautics, 2018, 35(1):84-93.

[14] JU J S, JIANG X G, FU X R. Elasto-plastic impact load of the beam subjected to lateral shock of ball

[J]. *Engineering Mechanics*, 2008(4):32-38.

- [15] XU B, ZENG X. Experimental study on the behaviors of reinforced concrete beams under impact loading [J]. *Journal of Civil Engineering*, 2014, 47(2): 41-51,61.
- [16] ZENG Xiang. Experimental and numerical study of behaviors of RC beams and columns under impact and rapid loading [D]. Changsha: Hunan University, 2014. (in Chinese)

Mr. **Zhou Danfa** received the B. S. degree in Aircraft Design and Engineering from Nanjing University of Aeronautics and Astronautics, Nanjing, China, in 2015. Now he is a postgraduate student in Aircraft Design at Nanjing University of Aeronautics & Astronautics.

Mr. **Ji Wenjie** received the B. S. degree in Aircraft Design

and Engineering from Nanjing University of Aeronautics and Astronautics, Nanjing, China, in 2015. Now he is a doctoral candidate in Mechanics at University of Science and Technology of China.

Mr. **Huang Boen** received the B. S. degree in Aircraft Design and Engineering from Nanjing University of Aeronautics and Astronautics, Nanjing, China, in 2015. After that, he entered Beihang University as a postgraduate student.

Mr. **Pei Houju** received the B. S. degree from Jiangsu University of Science and Technology in 2016. Now he is a doctoral candidate in Ergonomics and Environmental Engineering at Nanjing University of Aeronautics and Astronautics.

Mr. **Li Xinpeng** received the B. S. degree in Aircraft Design and Engineering from Nanjing University of Aeronautics and Astronautics, Nanjing, China, in 2015. Now he is a technical designer in Chengdu, China.

(Production Editor: Xu Chengting)